Global ubiquity of dynamic earthquake triggering

AARON A. VELASCO[1]*, STEPHEN HERNANDEZ[1], TOM PARSONS[2] AND KRIS PANKOW[3]

[1]Geological Sciences, University of Texas at El Paso, El Paso, Texas 79968, USA
[2]United States Geological Survey, Menlo Park, California 94025, USA
[3]University of Utah Seismograph Stations, Salt Lake City, Utah 84112, USA
*e-mail: velasco@geo.utep.edu

Published online: 25 May 2008; doi:10.1038/ngeo204

Earthquakes can be triggered by local changes in the stress field (static triggering[1–7]) due to nearby earthquakes or by stresses caused by the passage of surface (Rayleigh and Love) waves from a remote, large earthquake (dynamic triggering[8–18]). However, the mechanism, frequency, controlling factors and the global extent of dynamic triggering are yet to be fully understood. Because Rayleigh waves involve compressional and dilatational particle motion (volumetric changes) as well as shearing, whereas Love waves only involve shearing, triggering by either wave type implies fundamentally different physical mechanisms. Here, we analyse broadband seismograms from over 500 globally distributed stations and use an automated approach to systematically identify small triggered earthquakes—the low-amplitude signals of such earthquakes would normally be masked by high-amplitude surface waves. Our analysis reveals that out of 15 earthquakes studied of magnitude (M) greater than 7.0 that occurred after 1990, 12 are associated with significant increases in the detection of smaller earthquakes during the passage of both the Love and Rayleigh waves. We conclude that dynamic triggering is a ubiquitous phenomenon that is independent of the tectonic environment of the main earthquake or the triggered event.

Triggering of earthquakes has been classified into two primary areas of study: static and dynamic. Static triggering occurs within a few fault lengths of a mainshock rupture, and results from slip-induced changes in the local stress field[1–7]. Anomalous earthquake rate increases, associated with mainshock timing at distances beyond the influence of static stress increases, must be triggered by another process. These events, called dynamically (or remotely) triggered events, usually correlate with the passage of large-amplitude and long-duration transient signals: seismic surface waves[8].

Surface waves, usually the largest-amplitude arrivals on a seismogram, produce increased strain as they travel along the surface of the Earth. Surface-wave amplitudes can be highly impacted by the nature of an earthquake rupture, such as its depth, focal mechanism and rupture style (for example, directivity effects)[19,20]. Surface-wave propagation also contains dispersion, where velocities are a function of frequency. These waveforms are characterized by long durations, long periods (dominant periods ~20 s but range from several to hundreds of seconds) and emergent wave-train signals, as opposed to P and S waves, which are generally impulsive arrivals. Furthermore, small, local earthquakes recorded on a single station can be hidden within these frequency-dependent, large-amplitude signals. To investigate the role of surface waves in dynamic triggering, we used broadband seismograms from open network data (for example, Global Seismic Network, USArray and so on) available at the Incorporated Research Institutions for Seismology (IRIS) Data Management Center (DMC). Using this data set, we systematically determined the presence of small signals embedded within the surface-wave signals and documented the global extent of dynamically triggered earthquakes.

We identified triggered events using filtered broadband data optimized for the detection of small, local events near a seismic station. In particular, local events hidden in large-amplitude surface waves were detected by applying a high-pass filter to include frequencies greater than 5 Hz. Figure 1 shows displacement seismograms for the 26 December 2004 $M_w = 9.2$ Sumatra–Andaman islands earthquake recorded at station OTAV ($\Delta = 173°$) in Ecuador, which is located near the antipode off the coast of South America. The figure shows unfiltered Love and Rayleigh waves, plus the high-pass-filtered (corner at 5 Hz) vertical component of ground motion. Note the triggered event on the high-pass-filtered seismogram that occurs during the peak amplitude of the Rayleigh wave. This event is too small to be recorded in the global US Geological Survey Preliminary Determination of Epicenters catalogue. The Sumatra–Andaman islands earthquake triggered events at Mount Wrangell, Alaska, thousands of kilometres away from the epicentre[8], it triggered this event, and as we will show, it triggered events in many regions throughout the world.

Global catalogues generally detect and associate P waves from multiple stations to locate an event; thus, many small events with P waves recorded on fewer than 3–5 stations may not be located. This event criterion determines the detection threshold of a network, which is a direct result of the station coverage. For example, the US Geological Survey Preliminary Determination of Epicenters catalogue typically records earthquakes of $M \geq 4.5$ throughout the world, but this lower threshold varies depending on the global network station coverage. Regional catalogues, such as in California, Nevada, and Utah typically record much smaller ($M \sim 1$) events. Our approach is to detect small events near broadband stations using all data available from open sources, independent of global or regional catalogues.

To systematically identify small events typical of dynamic triggering, we developed an efficient and effective automated approach and systematically analysed data from 15 large to

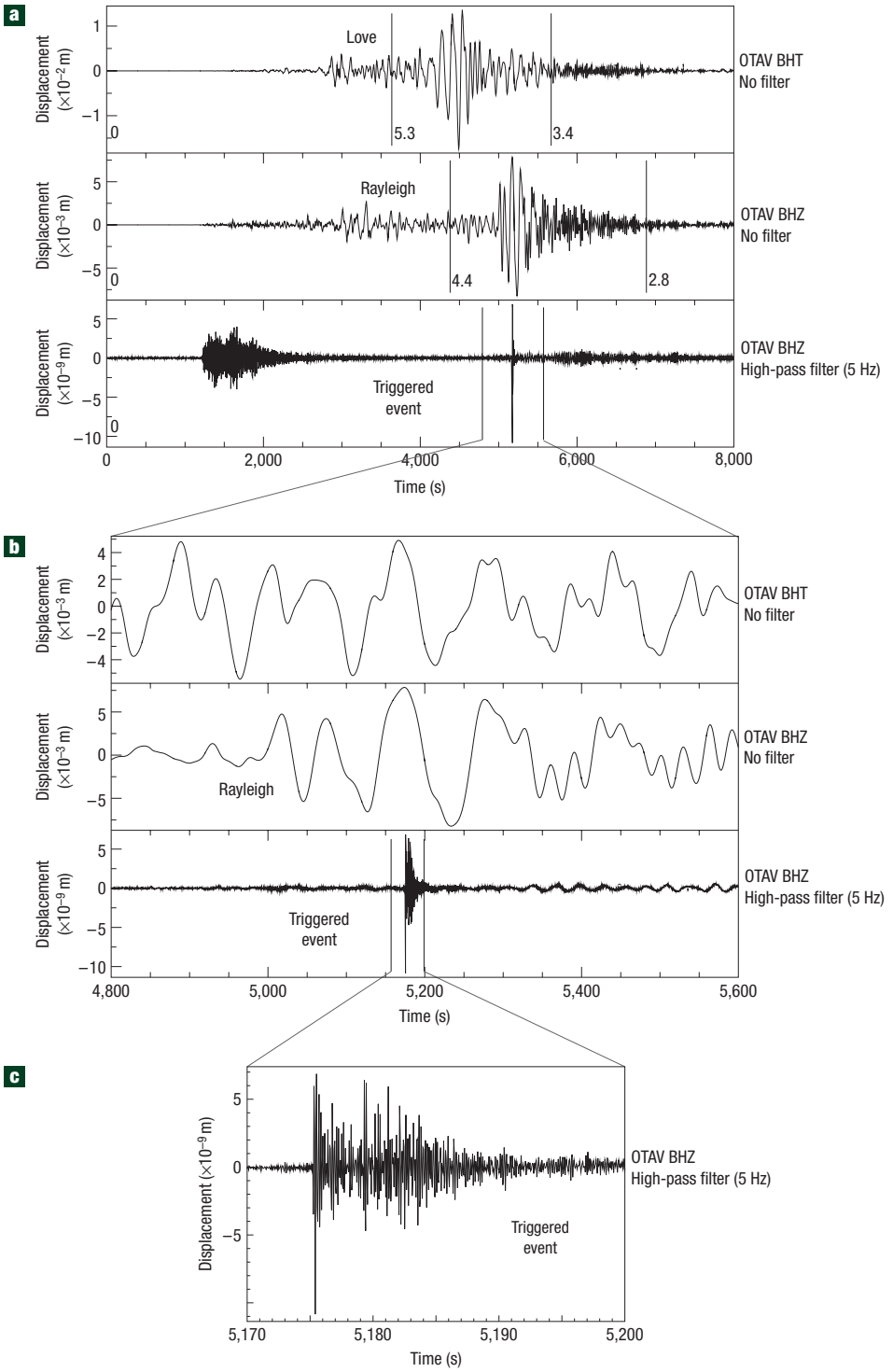

Figure 1 Transverse (BHT) and vertical (BHZ) displacement seismograms for the 26 December 2004, Sumatra ($M = 9.2$) earthquake. a, Recorded at the station in Otavalu, Ecuador, OTAV ($\Delta = 173°$), showing unfiltered Love and Rayleigh waves and the high-pass-filtered (at 5 Hz) vertical component. **b**, Same as in **a**, but with a reduced time (time divided by velocity) window showing the strong Rayleigh-wave arrival and the triggered event. **c**, Window of only the triggered event.

great size ($M > 7$) earthquakes that have occurred since 1990 (see Supplementary Information, Table S1; some of these earthquakes have already been attributed with causing dynamically triggered seismicity). The events occurred in a range of tectonic environments—many are strike–slip and show some form of directivity (unilateral, bilateral), suggesting a correlation between focal mechanism, directivity and triggering. For example, the 1999 Izmit event had a bilateral rupture[21] and triggered events from 400 to 1,000 km away from the epicentre[11], with the triggering being associated with the passage of the surface waves.

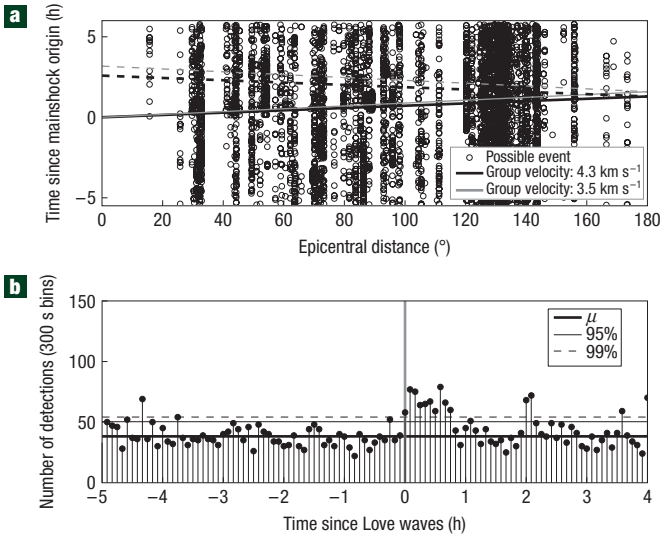

Figure 2 Detection map. a, Map showing possible triggered events recorded at 262 of 372 stations for the 2004 Sumatra–Andaman islands earthquake as recorded on each seismogram sorted by distance for all unclipped broadband data available at the DMC. Detections (circles) are plotted versus epicentral distance from the earthquake. Each detection is a potential local event. Solid lines represent short-arc surface-wave arrivals, and dashed lines represent long-arc arrivals. **b**, Histogram for detections summed along the Love-wave group velocity curve (4.3 km s^{-1}) using 300 s bins. The vertical grey line is the arrival of the Love wave, whereas the bold horizontal line represents the mean (μ) for the time period before the arrival of the Love wave. The other two horizontal lines, solid and dashed, show the 95% and 99% confidence bounds, respectively. Zero time on the histograms is the time of the Love-wave arrival. Note that there is a peak at time zero and a secondary peak near 7,000 s (~2 h) after the arrival of a short-arc Love wave (G1), which represents a cluster of events that occurred near the Nevada–California border, north of the Long Valley Caldera. Other peaks can be seen that we were unable to associate with any particular cluster.

We automated the detections of possibly triggered events by using the Antelope software (BRTT) to develop and apply a short-term average/long-term average (STA/LTA) detector on long-time-windowed (5 h before and after the origin time of the event), high-pass-filtered seismograms. We applied the STA/LTA detector to all on-scale vertical-component broadband data (requiring visual inspection of all data) for the events listed in Supplementary Information, Table S1, collected from the IRIS DMC. Then, we optimized the detector to identify local events (adjusting window lengths for the STA and LTA and placing a strict detection criterion of 3.5 for the STA/LTA)[22] and plotted detections versus epicentral distance (Fig. 2). However, many of the detections may be untriggered 'natural' events—exotic events, such as non-volcanic tremors[23], mining explosions or other man-made activity. To systematically demonstrate that triggering occurs during the passage of the surface waves, we summed detections along the group velocity curves for Love waves, creating Love-wave velocity, time-reduced histograms for detections using 300 s bins (Fig. 2b). We then computed a mean number of detections before the origin time for reference.

Activity that increases with the arrival of seismic waves is more confidently identified as triggered. For the Sumatra–Andaman islands earthquake (Fig. 2), we found a peak at time zero and a secondary peak near 7,000 s after the arrival of a short-arc Love wave (G1). The secondary peak is a cluster of events ($M < 2.5$) that occurred near the Nevada–California border, in a commonly active area north of the Long Valley Caldera (Nevada Seismological Laboratory Catalog (NSLC)). The events, all with $M < 2.5$ (NSLC), occurred well after the arrival of the surface waves associated with the Sumatra–Andaman islands earthquake. However, differentiating between triggered versus 'natural' events is challenging with this delay. In Fig. 2a, the number of detections becomes so numerous that the figure becomes saturated at a distance between 120 and 130°, which corresponds to North American stations for this event. Many stations may have multiple detections, that on inspection, can be attributed to high-frequency noise—from human disturbances, passing vehicles, radio towers and so on. As we lack intricate details for each station and to account for noisy stations, we eliminated stations with more than 100 detections per station over the 10 h of data. Furthermore, we eliminated stations within 10° of the epicentre (this was extended to 20° for the Sumatra–Andaman islands earthquake owing to the rupture length) to remove bias caused by the detection of aftershocks. This also guaranteed that remotely triggered events were obtained.

To test the significance of the number of detections that occurred after the passage of the surface waves, we computed the average number of detections that occurred in the 300 s bins before time zero. Approximating a Poisson distribution, we computed the 95% and 99% confidence intervals. If the number of detections surpassed the 99% confidence interval, we consider this bin to exhibit triggering characteristics, or to be non-random. Many of these possibly triggered events are not in the global, regional or local earthquake catalogues; thus, for many of these previously undetected events, we do not know their location nor their focal mechanism. Our approach does not locate these small, triggered events, nor are locations crucial for our results. However, the NSLC locations for the cluster following the Sumatra–Andaman islands earthquake give us confidence that (1) our approach detects a large number of small events, (2) our approach is sensitive to small events ($M < 3.0$) and (3) this method enables global detection of small events that are near broadband stations.

Love-wave velocity, time-reduced histograms for 12 of the 15 $M > 7$ earthquakes show significant remote triggering (see Supplementary Information, Table S2). Only the Hector Mine, Siberia and Kuril events lack a significant triggering detection signal beyond 10°. The 1992 Landers, 1999 Hector Mine and 2002 Denali Fault earthquakes were previously shown to have dynamic triggering. The Landers and Denali Fault earthquakes clearly show a peak after the passage of the Love wave (time 0), whereas the Hector Mine earthquake shows no triggering signal. Although the Hector Mine earthquake did not trigger events beyond 10°, remote triggering was reported much closer[24]. To summarize the results over all earthquakes, we stacked the number of detections for all events (Fig. 3a). The mean number of earthquakes detected globally was 609 ± 73 (95% confidence) in the 5 h window before the arrival of the Love waves. A significant increase (above 95% confidence) occurs with the arrival of the surface waves and persists for at least 0.8 h (48 min.). After the initial Love-wave arrival, the local earthquake rate increased 37% above mean background (Fig. 3b); following the Rayleigh-wave arrivals the rate increased 60% above the background (Fig. 3c). The proportion of triggered earthquakes caused by each phase is difficult to untangle because of dispersion and the events associated with Rayleigh-wave arrivals could be the result of secondary triggering from the Love-wave events preceding them. These results suggest that both surface-wave phases trigger tectonic earthquakes around the world.

The sensitivity of detection is also important because a single cluster recorded on a few stations can dominate any result, especially if the cluster occurs within a densely stationed region,

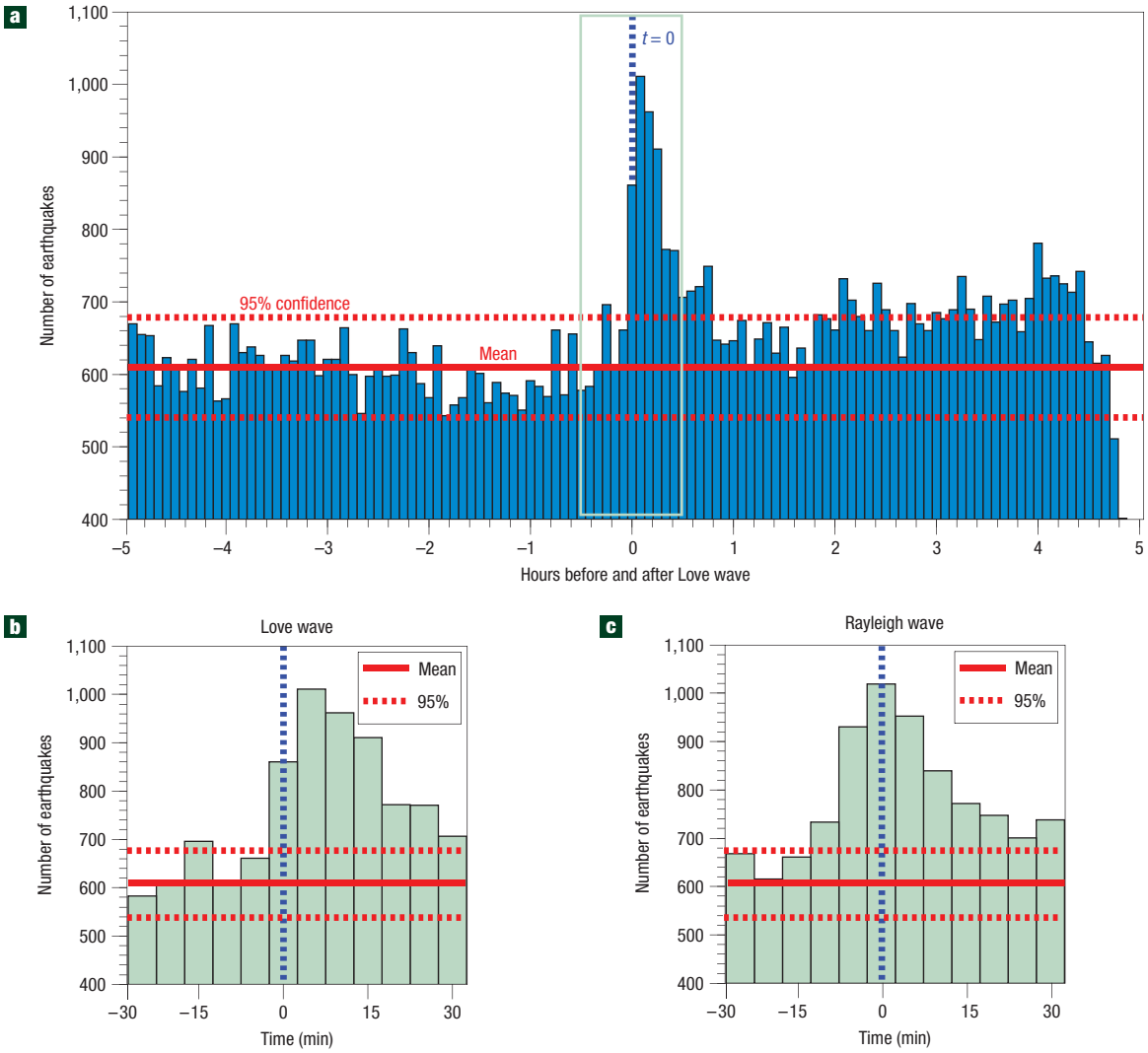

Figure 3 Histograms of stacked detections for all 15 mainshocks in this study. a, Detection of remote earthquakes, stacked in 300 s bins, that occurred within 5 h before/after the expected Love-wave arrival. The mean number of local earthquakes detected globally is 609 ± 73 (95% confidence) in the period before Love waves arrived at stations. A rate increase above 95% confidence on background is associated with surface-wave arrivals that persisted for at least 0.8 h. **b**, Close-up of the outlined area from **a**, showing that globally, Love-wave arrivals cause a 37% local earthquake rate increase above mean background. **c**, By the arrival of the Rayleigh waves, the global rate increases reached 60% above background.

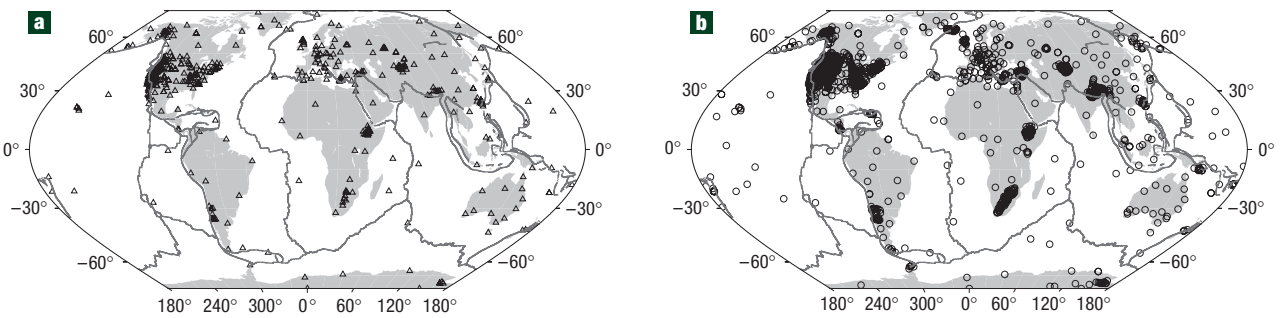

Figure 4 Maps showing stations and detection rates. a, Stations shown with triangles had a doubling of their detection rate after the passage of the surface waves. **b**, Circles identify stations that showed no increase. The global distribution of triggering suggests that dynamic triggering is independent of the tectonic environment.

in which case, the multiple stations compound the number of events in our detection map. We determined whether a few stations dominate the histograms by calculating the average detection rate for each station before the origin time of the arrival of the surface wave. If a station showed a doubling in the detection rate after the arrival of the surface wave in the first three bins, we considered the station triggered. Our approach was similar to the STA/LTA approach for arrival detection, which takes into account typical background detection rates at a single station. The percentages of triggered stations for all events range between 15 and 30% (Supplementary Information, Table S2 gives numbers and percentages for all events). No single station or network disproportionately skewed our results. Figure 4 shows all stations that exhibit a doubling of the detection rate for all 15 events studied. Many stations show triggering in a wide variety of tectonic environments, from stable cratons to active margins.

In sum, 12 of 15 post-1990 $M > 7.0$ earthquakes showed significant increases in the number of detections during the passage of both the Love and Rayleigh waves. Furthermore, over 500 stations throughout the world that sit in different tectonic settings showed a doubling of the detection rate after the passage of the surface wave for these 15 events. Thus, we conclude that dynamic triggering occurs frequently as a result of the passage of both Rayleigh and Love waves, and is independent of the tectonic environment of the triggered event and the mainshock. Our results also suggest that a number of physical mechanisms must play a role in dynamic triggering.

Received 8 January 2008; accepted 22 April 2008; published 25 May 2008.

References

1. King, G. C. P., Stein, R. S. & Lin, J. Static stress changes and the triggering of earthquakes. *Bull. Seismol. Soc. Am.* **84**, 935–953 (1994).
2. Stein, R. S., King, G. C. P. & Lin, J. Stress triggering of the 1994 $M = 6.7$ Northridge, California, earthquake by its predecessors. *Science* **265**, 1432–1435 (1994).
3. Harris, R. A., Simpson, R. W. & Reasenberg, P. A. Influence of static stress changes on earthquake locations in southern California. *Nature* **375**, 221–224 (1995).
4. Harris, R. A. & Simpson, R. W. In the shadow of 1857—The effect of the great Ft. Tejon earthquake on subsequent earthquakes in southern California. *Geophys. Res. Lett.* **23**, 229–232 (1996).
5. Harris, R. A. Introduction to special section: Stress triggers, stress shadows, and implications for seismic hazard. *J. Geophys. Res.* **103**, 24347–24358 (1998).
6. Parsons, T. Global Omori law decay of triggered earthquakes: Large aftershocks outside the classical aftershock zone. *J. Geophys. Res.* **107**, doi:10.1029/2001JB000646 (2002).
7. Lin, J. & Stein, R. S. Stress triggering in thrust and subduction earthquakes and stress interaction between the southern San Andreas and nearby thrust and strike-slip faults. *J. Geophys. Res.* **109**, doi:10.1029/2003JB002607 (2004).
8. West, M., Sanchez, J. J. & McNutt, S. R. Periodically triggered seismicity at Mount Wrangell, Alaska, after the Sumatra earthquake. *Science* **308**, 1144–1146 (2005).
9. Anderson, J. G. *et al.* Seismicity in the western Great Basin apparently triggered by the Landers, California earthquake, 28 June 1992. *Bull. Seismol. Soc. Am.* **84**, 863–891 (1994).
10. Hill, D. P. *et al.* Seismicity in the western United States remotely triggered by the M 7.4 Landers, California, earthquake of June 28, 1992. *Science* **260**, 1617–1623 (1993).
11. Brodsky, E. E., Karakostas, V. & Kanamori, H. A new observation of dynamically triggered regional seismicity: earthquakes in Greece following the August, 1999 Izmit, Turkey earthquake. *Geophys. Res. Lett.* **27**, 2741–2744 (2000).
12. Gomberg, J., Bodin, P., Larson, K. & Dragert, H. Earthquake nucleation by transient deformations caused by the $M = 7.9$ Denali, Alaska, earthquake. *Nature* **427**, 621–624 (2004).
13. Pankow, K. L., Arabasz, W. J., Pechmann, J. C. & Nava, S. J. Triggered seismicity in Utah from the November 3, 2002, Denali Fault earthquake. *Bull. Seismol. Soc. Am.* **94**, S332–S347 (2004).
14. Prejean, S. G. *et al.* Remotely triggered seismicity on the United States west coast following the M 7.9 Denali Fault earthquake. *Bull. Seismol. Soc. Am.* **94**, S348–S359 (2004).
15. Husen, S., Wiemer, S. & Smith, R. B. Remotely triggered seismicity in the Yellowstone National Park region by the 2002 $M_w = 7.9$ Denali Fault Earthquake, Alaska. *Bull. Seismol. Soc. Am.* **94**, S317–S331 (2004).
16. Eberhart-Phillips, D. *et al.* The 2002 Denali fault earthquake, Alaska: A large magnitude, slip-partitioned event. *Science* **300**, 1113–1118 (2003).
17. Husker, A. L. & Brodsky, E. E. Seismicity in Idaho and Montana triggered by the Denali Fault Earthquake: A window into the geologic context for seismic triggering. *Bull. Seismol. Soc. Am.* **94**, S310–S316 (2004).
18. Hill, D. P. Dynamic stresses, Coulomb failure, and remote triggering. *Bull. Seismol. Soc. Am.* **98**, 66–92 (2008).
19. Velasco, A. A., Ammon, C. J., Farrell, J. & Pankow, K. Rupture directivity of the November 3, 2002 Denali Fault earthquake determined from surface waves. *Bull. Seismol. Soc. Am.* **94**, S293–S299 (2004).
20. Velasco, A. A., Ammon, C. J. & Lay, T. Empirical Green function deconvolutions of broadband surface waves: Rupture directivity of the 1992 Landers, California ($M_w = 7.3$) earthquake. *Bull. Seismol. Soc. Am.* **84**, 735–750 (1994).
21. Li, X., Cormier, V. F. & Toksöz, M. N. Complex source process of the 17 August 1999 Izmit, Turkey, earthquake. *Bull. Seismol. Soc. Am.* **92**, 267–277 (2002).
22. Steck, L., Velasco, A. A., Cogbill, A. H. & Patton, H. J. Improving regional seismic event location in China. *Pure Appl. Geophys.* **158**, 211–240 (2001).
23. Rubenstein, J. L. *et al.* Non-volcanic tremor driven by large transient shear stresses. *Nature* **448**, 579–582 (2007).
24. Gomberg, J. & Johnson, P. Dynamic triggering of earthquakes. *Nature* **437**, 830 (2005).

Supplementary Information accompanies this paper on www.nature.com/naturegeoscience.

Acknowledgements

S.H. was supported by a grant from the National Science Foundation (GEO 0503610). The facilities of the IRIS Data Management System, and specifically the IRIS DMC, were used to access the waveform data and metadata required in this study. The IRIS Data Management System is funded through the NSF and specifically the GEO Directorate through the Instrumentation and Facilities Program of the NSF under Cooperative Agreement EAR-0552316. Comments by D. Kilb significantly improved this manuscript.

Author information

Reprints and permission information is available online at http://npg.nature.com/reprintsandpermissions. Correspondence and requests for materials should be addressed to A.A.V.